# Highly Dense, Transparent-Al2O3 Ceramics From Ultrafine Nanoparticles Via a Standard SPS Sintering

Nicolas Roussel, Lucile Lallemant, Jean-Yves Chane-Ching, Sophie Guillemet-Fristch, Bernard Durand, Vincent Garnier, Guillaume Bonnefont, Gilbert Fantozzi, Lionel Bonneau, Sandrine Trombert, et al.

# Highly Dense, Transparent $\alpha$-$Al_2O_3$ Ceramics From Ultrafine Nanoparticles Via a Standard SPS Sintering

Nicolas Roussel,[‡] Lucile Lallemant,[§] Jean -Yves Chane-Ching,[‡,†] Sophie Guillemet-Fristch,[‡] Bernard Durand,[‡] Vincent Garnier,[§] Guillaume Bonnefont,[§] Gilbert Fantozzi,[§] Lionel Bonneau,[¶] Sandrine Trombert,[¶] and Domingo Garcia-Gutierrez[‖]

[‡]Université de Toulouse, CNRS-UPS-INPT, CIRIMAT, 118 Route de Narbonne, Toulouse 31062, France

[§]Université de Lyon, CNRS-INSA Lyon, MATEIS, Villeurbanne 69621, France

[¶]Baikowski, Les Marais Noirs Ouest, BP 501, La Balme de Sillingy 74339, France

[‖]Centro de Innovacion, Investigacion y Desarrollo en Ingenieria y Tecnologia, UANL, Carretera al Aeropuerto, Apodaca, Nuevo Leon, Mexico

**Using discrete, ultrafine alumina, highly dense transparent (71% real in-line transmission, RIT, $\lambda$ = 640 nm) ceramics were achieved with grain size as small as 260 nm using standard SPS sintering. We show that use of $La^{3+}$ as a dopant greatly reduces sensitivity to the sintering temperatures. Transparent alumina were achieved in a large range of sintering temperatures, 1140°C < *T* < 1200°C, thus providing better reliability and flexibility into the fabrication of large sintered transparent ceramic bodies.**

## I. Introduction

Dense, refractory transparent ceramics are of technological importance in high-temperature light transmitting materials,[1] armor,[2] IR emitters envelopes,etc[3] Indeed, ideal process routes to the fabrication of such materials will involve use of ultrafine nanoparticles along specific forming and sintering process routes. Large-scale development of such materials has been hindered by the availability of discrete, refractory nanoparticles. Their synthesis represents a challenging task face to the high driving force for sintering and coarsening existing at the high temperatures required for structure crystallization of the nanocrystals. In this context, highly transparent alumina ceramics were developed[4–7] because they combine transparency and high mechanical properties. Indeed, sintered transparent $\alpha$-$Al_2O_3$ ceramics displaying RIT values of 72% ($e$ = 0.8 mm)[2] were achieved in a two-step process route including presintering under vacuum to close porosity followed by final densification using hot isostatic pressing. Another interesting transparent alumina ceramic displaying a real in-line transmission of ~69% ($e$ = 0.80 mm)[6] was obtained by high-pressure spark plasma sintering involving a uniaxial pressure of 400 MPa and an in-house experimental setup including graphite dies and WC disks. Because the best results to date require sintering processes involving several stages or specific conditions, fabrication of transparent alumina through standard densification process route is highly desirable.

With this objective, routine fabrication of transparent alumina ceramic requires availability of ultrafine $Al_2O_3$ nanocrystals with controlled physicochemical properties. Various process routes were recently proposed for the fabrication of ultrafine refractory nanoparticles.[8,9] Indeed, discrete, $\alpha$-$Al_2O_3$ ultrafine nanoparticles were recently developed and commercialized. Here, we show that using discrete, ultrafine highly pure $\alpha$-$Al_2O_3$ nanoparticles, careful control of feature characteristics such as surface chemistry, interparticle interactions during green body forming, and grain growth during sintering will allow the formation of highly dense $\alpha$-$Al_2O_3$ transparent ceramic through standard SPS sintering technique. Interestingly, using a specific dopant addition procedure, we demonstrate that $La^{3+}$, a dopant previously used to improve transmittance of transparent $Al_2O_3$ ceramics,[10,11] enlarges the temperature range for achieving high RIT values, providing higher flexibility for the fabrication of transparent refractory alumina ceramics.

## II. Experimental Procedure

Baikowski provided $\alpha$-$Al_2O_3$ nanoparticles aqueous slurries ($D^n_{50}$ = 80 nm) . The as-received slurries were centrifuged and redispersed in demineralized $H_2O$. Control experiments were carried out using a commercial $\alpha$-$Al_2O_3$ dispersion displaying polycrystalline nanoparticles with an average size of $D^n_{50}$ = 140 nm. Particle size measurements were made using a Mastersizer 2000 (Malvern, Worcestershire, UK) laser diffraction particle size analyzer.

The $La^{3+}$ doping of $\alpha$-$Al_2O_3$ nanoparticles was performed by adding $La(NO_3)_3$ 6 $H_2O$ on a concentrated $Al_2O_3$ slurry (53 wt% $\alpha$-$Al_2O_3$, $d$ = 1.6) yielding a 0.1$M$ $La^{3+}$ concentration. After room-temperature stirring overnight, the slurry was centrifuged at 2000 G and redisperse into demineralized $H_2O$ with a final 68 wt% $Al_2O_3$, $d$ = 1.95. A doping concentration of 480 atomic ppm (ppma) $La^{3+}$ was determined by ICP analysis on the resulting dispersion. TEM observation of the nanocrystals was performed on the purified dispersions using a JEOL JEM 1011 (JEOL, Tokyo, Japan). HRTEM was carried out on samples prepared from a small volume of sample (6–7 μL) deposited on a lacey carbon membrane supported on TEM copper grids, followed by room-temperature drying. Images were recorded at 200 KV on a FEI TITAN G2 60–300 microscope (FEI Europe, Eindhoven, the Netherlands).

High-density green compact ($D$ = 20 mm) was achieved using a liquid forming procedure.[12] The slurry was slip cast

A. Krell—contributing editor

onto 20 mm diameter porous alumina molds to avoid any contamination. All the green bodies were manually polished to obtain 2 g cylindrical samples.

Densification of the resulting compacts was performed using a standard SPS technique (HP D 25/1, FCT System, Rauenstein, Germany). Samples were sintered with the following cycle: applied uniaxial pressure of 80 MPa throughout the cycle, rapid heating up to 800°C, heating rate of 10°C/min from 800°C to 950°C followed by a slower heating rate (1°C/min) up to the final sintering temperatures. The final sintering temperature was in the 1060°C–1200°C range.

After sintering, the samples ($D$ = 20 mm) were carefully mirror-polished on both sides using diamond slurries (to 1 μm) and the transparency in the center of the pellet (spot size 5 mm × 2 mm) was determined by a (Jasco V-670, JASCO Easton, MD). Real in-line transmittance (RIT) measurements were conducted using a shield with an appropriate aperture placed between the sample and the detector to avoid scattered light with angle > 0.5°. All the RIT values reported in this article were measured for λ = 640 nm and the RIT were normalized at similar thickness of $t_2$ = 0.80 mm using the following equation RIT ($t_2$) = $(1-R_S)$ $[(\mathrm{RIT}(t_1)/(1-R_S)]^{t2/t1}$ where $R_S$ denote the total normal surface reflectance (0.14 for transparent alumina), RIT ($t_i$) is the RIT for a sample of thickness $t_i$.

## III. Results and Discussion

### *(1) α-$Al_2O_3$ Ultrafine Nanoparticles and Dispersion Properties*

Highly pure α-$Al_2O_3$ nanoparticles dispersions were prepared by $HNO_3$ peptization followed by post purification using ultracentrifugation and redispersion. Consistently, increased repulsive interparticle interactions as revealed from zeta potential measurement are achieved from complete removal of the residual $Al^{3+}$ cations from the dispersions. Thus, highly concentrated α-$Al_2O_3$ dispersions displaying volume fractions, $\Phi_v$ up to 0.33 were obtained due to the high degree of nanoparticles individualization.

A similar approach was adopted to the preparation of highly individualized $La^{3+}$-doped α-$Al_2O_3$ nanoparticle dispersions. Fine tuning of the interparticle interactions involves absorption of $La^{3+}$ cations on α-$Al_2O_3$ nanoparticles surfaces followed by post removal of the non absorbed $La^{3+}$ cations from the dispersions. Although divalent and trivalent metal cation do not exhibit a high absorption affinity to the $Al_2O_3$ surface in the pH range, 3 < pH < 4,[13] a $La^{3+}$ dopant concentration of 120 atomic ppm (ppma) corresponding to a surface coverage ratio of 0.01 was achieved by contacting a 0.1$M$ $La^{3+}$ solution and post removal of the residual $La^{3+}$ by centrifugation at 2000 G. Likewise, stable, highly concentrated of $La^{3+}$-doped α-$Al_2O_3$ nanoparticles dispersions displaying concentration up to $\Phi_v$ = 0.30 were prepared.

High purity of these nanoparticles was shown by characterizations performed on solids after $H_2O$ room-temperature evaporation from the dispersions. Chemical analysis reveals low impurity content (Na = 10 ppm, K = 15 ppm, Fe = 7 ppm Si = 18 ppm, Mg = 10 ppm, Ca = 5 ppm). X-ray diffraction performed on dried powder shows peaks attributed to the α-$Al_2O_3$ structure without any trace of the γ-$Al_2O_3$. Ordered domains of 58 nm were determined from [012], [104], [110], and [113] diffraction peaks using Debye-Scherer formula.

A monodisperse size distribution and a mean hydrodynamic diameter of 80 nm were determined on the pure and $La^{3+}$-doped α-$Al_2O_3$ dispersions by dynamic light scattering. In contrast to the reference powder [Fig. 1(d)], TEM investigation reveals discrete nanoparticles exhibiting isotropic morphology with an average size of 80 nm [Fig. 1(a)]. This average size, slightly larger than the XRD ordered domain suggests that the α-$Al_2O_3$ nanoparticles are indeed composed of a few number of primary crystallites. HRTEM image

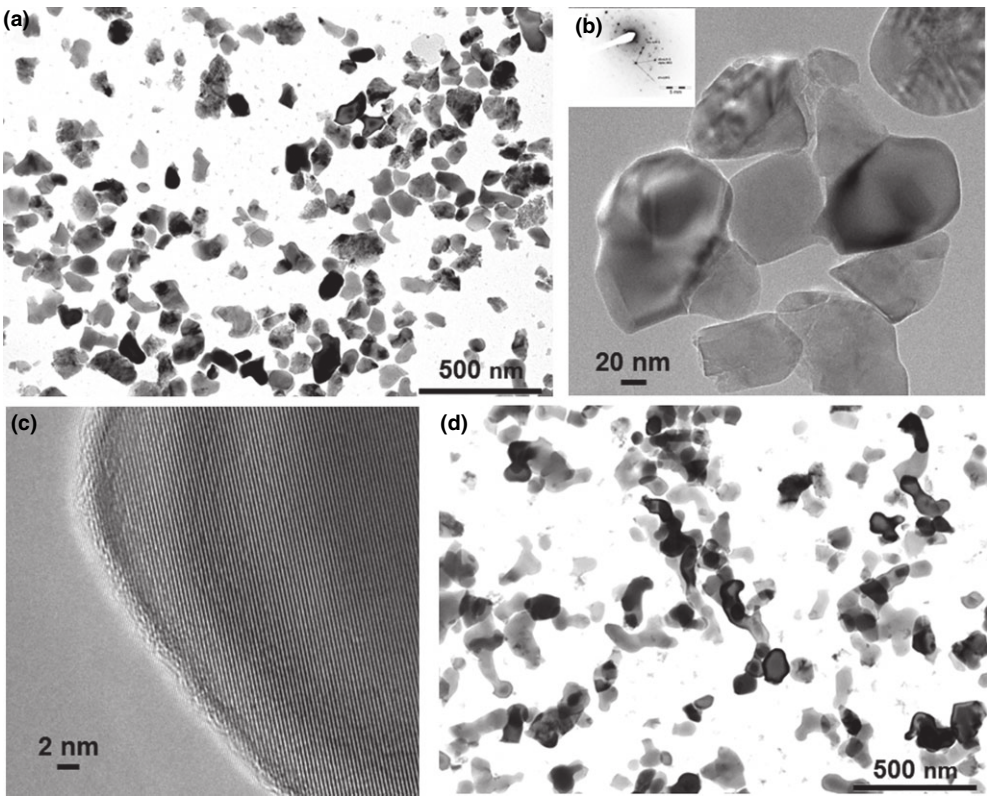


**Fig. 1.** TEM images of α-$Al_2O_3$ nanoparticles. (a) Low magnification image showing perfectly discrete $Al_2O_3$ nanoparticles. (b) High magnification TEM images showing primary crystallites of 80 nm. Inset: Electronic diffraction pattern showing crystalline α-$Al_2O_3$ structure. (c) HRTEM image revealing highly crystallized interface. (d) Low magnification image of a reference powder showing non-isotropic aggregated particles.

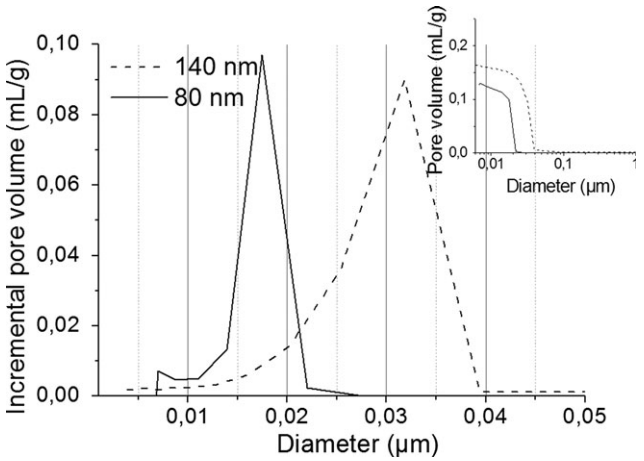


**Fig. 2.** Pore diameter distribution of $\alpha$-$Al_2O_3$ green body formed from 80 nm nanoparticles showing monodisperse pore distribution and a mean pore diameter of 18 nm. Pore distribution of the reference powder (140 nm) is also given for comparison. Inset: Pore volume suggesting a higher green density when using discrete, isotropic ultrafine $\alpha$-$Al_2O_3$ nanoparticles.

[Fig. 1(b)] clearly reveals that the nanoparticles are monocrystalline or composed of a few number of primary crystallites.

Because sintering involves surface and grain-boundary diffusion,[14] the $\alpha$-$Al_2O_3$ nanoparticle surface was fully characterized. Indeed, peptization of nanosized $\alpha$-$Al_2O_3$ usually leads to formation of Al polycations. Although pH of the resulting dispersions was determined around pH 3.75, no trace of $Al_{13}O_4(OH)_{24}(H_2O)_{12})^{7+}$ polymer was detected by $^{27}Al$ liquid NMR performed on these dispersions indicating no significant surface deterioration of $\alpha$-$Al_2O_3$ nanoparticles after $HNO_3$ peptization. The well crystalline character of the $\alpha$-$Al_2O_3$ surfaces was confirmed through a HRTEM investigation showing perfectly crystallized interface observed without presence of any amorphous phase [Fig. 1(c)].

### *(2) Forming, Sintering and Optical Properties*

Forming of the green body was carried out by slip casting from the concentrated dispersions. Hg porosimetry performed on green compacts reveals a quasi-monodisperse pore size distribution with a mean pore diameter of 18 nm (Fig. 2). Interestingly, a green density of 58% is achieved on compacts formed from these individualized nanoparticles. Note that the reference sample composed of nanoparticles displaying a less isotropic morphology exhibits a lower green density, larger pore size distribution and a much higher mean pore size value of 32 nm.

Sintering of the slip-cast green bodies was performed by standard SPS sintering. Our temperature profile was designed with the objective to achieve full densification while inhibiting grain growth. Although activation energy of densification is generally higher than that of grain growth[14] our temperature profile involves a rather low densification temperature associated with a low heating rate.[15] Indeed, heating rates were shown to strongly influence the spark plasma sintering mechanism of $\alpha$-$Al_2O_3$ and grain coarsening was greatly minimized when sintering using the designed temperature profile. Highest RIT values of the non-doped (RIT = 68%) and $La^{3+}$-doped (RIT = 71%) $\alpha$-$Al_2O_3$ compacts were achieved at 1100°C and 1140°C [Fig. 3(a)], respectively. To the best of our knowledge, these values are the highest values obtained in standard SPS sintering. As lower RIT values, RIT = 53% were obtained in similar forming and sintering conditions[12] using the reference powder, characteristic features of the ultrafine $\alpha$-$Al_2O_3$ powder such as ultrafine size, size monodispersity, and isotropic morphology are crucial parameters facilitating the formation of $\alpha$-$Al_2O_3$ transparent ceramics.

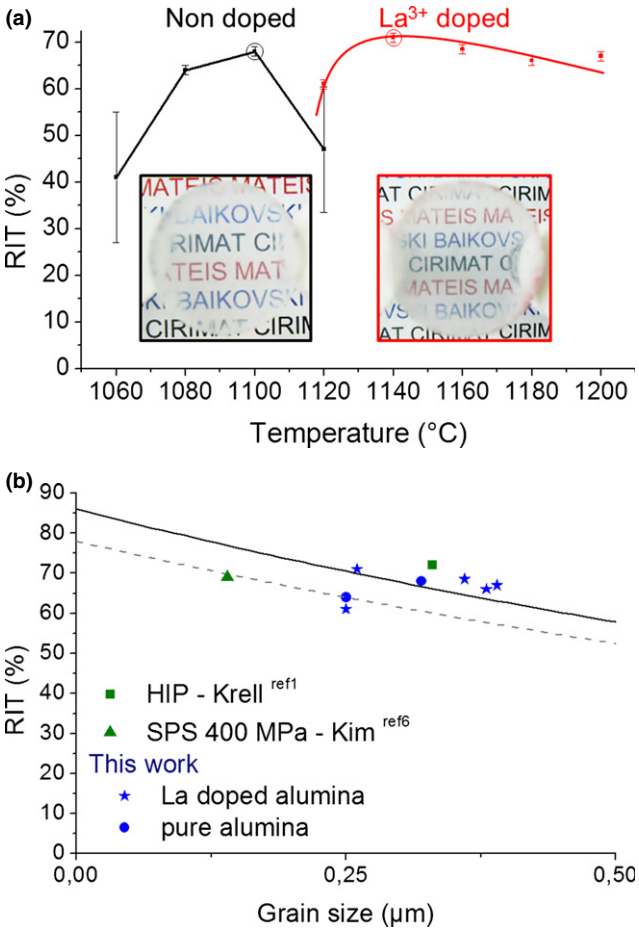


**Fig. 3.** (a) Dependence of RIT of nondoped and $La^{3+}$-doped sintered $\alpha$-$Al_2O_3$ on sintering temperature showing a larger range of densification temperatures with $La^{3+}$ dopant. Inset: photographs of samples taken at 2.8 cm above the text (i) non-doped sample sintered at 1100°C. (ii) $La^{3+}$-doped sample sintered at 1140°C. (b) RIT and grain size of sintered alumina. RIT model curves calculated from Ref. 1 versus grain size are reported suggesting full densification of our sintered $\alpha$-$Al_2O_3$. The model curves (continuous line: 0.00 vol% porosity, dotted line: 0.01 vol% porosity) were obtained with an average refractive index change $\Delta n = 0.005$ with a pore diameter = 100 nm. RIT values from literature were renormalized for $e = 0.80$ mm.

Comparison of our experimental RIT values to theoretical RIT[1] values determined at different grain sizes [Fig. 3(b)] suggests a full densification for the compacts sintered at 1100°C for the nondoped samples. Using the same argument, $La^{3+}$-doped samples sintered between 1140°C and 1200°C display full densification. Indeed, a higher sintering temperature[16] was observed for the $La^{3+}$-doped samples indicating diffusion blocking in the presence of $La^{3+}$. Note that this shift in sintering temperature for the $La^{3+}$-doped $\alpha$-$Al_2O_3$ material was previously observed in natural sintering. This shift was attributed[14] to reduced grain-boundary diffusivity arising from strong segregation of $La^{3+}$ to the grain boundary. From a HRTEM investigation carried out on $La^{3+}$-doped $\alpha$-$Al_2O_3$ materials at various $La^{3+}$ content, a similar effect of the $La^{3+}$ dopant in $\alpha$-$Al_2O_3$ spark plasma sintering was found. Indeed, presence of secondary phase $LaAl_{11}O_{18}$ at triple junction and along some grain boundaries was only observed on samples doped at high $La^{3+}$ content (600 ppma) while no inclusion was observed on samples doped below that concentration.

More interestingly, compared with the non-doped samples, a larger plateau of sintering temperatures yielding RIT values higher than 67% was observed with $La^{3+}$ dopant. Although similar RIT values were determined in the range of sintering

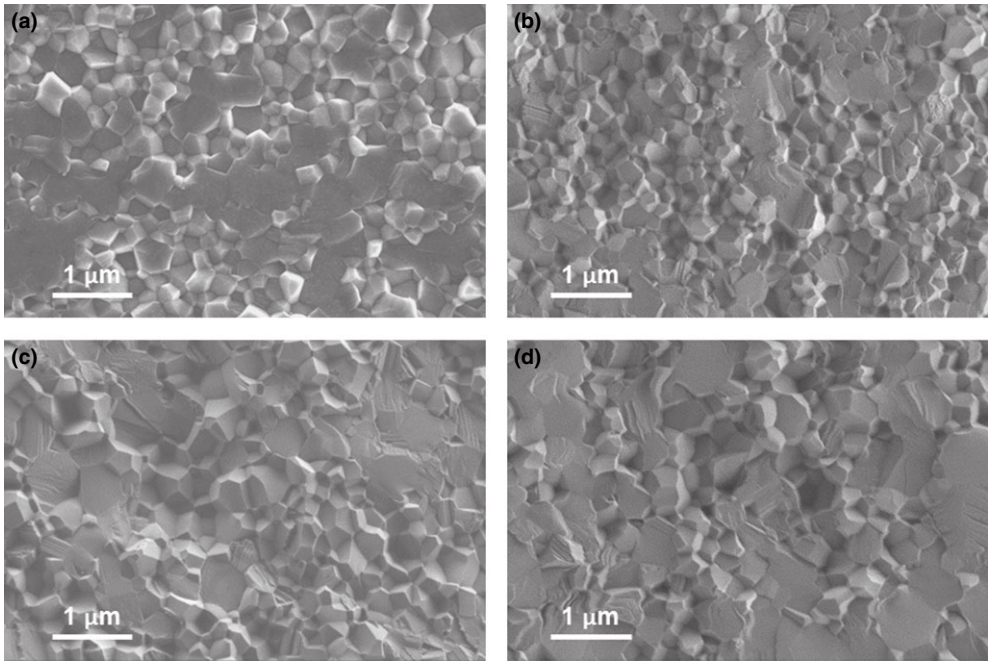


**Fig. 4.** SEM images showing pure and $La^{3+}$-doped $\alpha$-$Al_2O_3$ microstructures. (a) nondoped $Al_2O_3$ sintered at 1100°C, (b) $La^{3+}$-doped $\alpha$-$Al_2O_3$ sample sintered at 1140°C, (c) 1160°C, (d) 1200°C.

temperatures, 1140°C < $T$ < 1200°C, fine inspection of the corresponding microstructures [Fig. 4(a)] reveals a grain growth with average grain sizes ranging from 260 to 390 nm with increased sintering temperature. In contrast, a smaller window of sintering temperatures, 1080°C < $T$ < 1100°C, was determined for non-doped materials. Indeed, for these latter samples sintered at 1060°C and 1120°C, large variations of RIT values were observed inside a same sample, depending on the region investigated. These variations of RIT values were shown to arise from different grain size probably due to slight local variations of green density. All these observations highlight the beneficial use of $La^{3+}$ reducing sensitivity to sintering temperature.

From these results, future work aimed to the fabrication of high RIT transparent $\alpha$-$Al_2O_3$ ceramics will involve dispersion of agglomerate-free, mono-crystalline, ultrafine, $La^{3+}$-doped $\alpha$-$Al_2O_3$ building blocks.

## IV. Conclusions

Highly dense transparent (RIT 71%) $\alpha$-$Al_2O_3$ ceramics were achieved using discrete, ultrafine high purity $\alpha$-$Al_2O_3$ nanoparticles sintered by standard SPS technique. Crucial effects of the nanoparticle characteristics, such as size monodispersity, isotropic morphology, and surface chemistry were emphasized. We demonstrate the beneficial use of $La^{3+}$ as a dopant, reducing the sensitivity of sintering temperature, thus increasing flexibility to fabricate large homogenous transparent $\alpha$-$Al_2O_3$ ceramics.

## Acknowledgments

The authors acknowledge support from the Agence Nationale pour la Recherche, ANR, France. This work was done through the CERATRANS project.

## References

[1]R. Apetz and M. P. B. van Bruggen, "Transparent Alumina: A Light-Scattering Model," *J. Am. Ceram. Soc.*, **86** [3] 480–6 (2003).
[2]A. Krell, J. Klimke, and T. Hutzler, "Advanced Spinel and Sub- μm $Al_2O_3$ for Transparent Armour Applications," *J. Eur. Ceram. Soc.*, **29**, 275–81 (2009).
[3]A. Krell, T. Hutzler, and V. Klimke, "Transmission Physics and Consequences for Materials Selection, Manufacturing, and Applications," *J. Eur. Ceram. Soc.*, **29**, 207–21 (2009).
[4]A. Krell, J. Klimke, and T. Hutzler, "Transparent Compact Ceramics: Inherent Physical Issues," *Opt. Mater.*, **31** [1] 144–50 (2009).
[5]S. Grasso, B. N. Kim, C. Hu, G. Maizza, and Y. Sakka, "Highly Transparent Pure Alumina Fabricated by High-Pressure Spark Plasma Sintering," *J. Am. Ceram. Soc.*, **93** [9] 2460–2 (2010).
[6]B. N. Kim, K. Hiraga, S. Grasso, K. Morita, H. Yoshida, H. Zhang, and Y. Sakka, "High-Pressure Spark Plasma Sintering of MgO-Doped Transparent Alumina," *J. Ceram. Soc. Jap.*, **120** [3] 116–8 (2012).
[7]M. Stuer, Z. Zhao, U. Aschauer, and P. Bowen, "Transparent Polycrystalline Alumina Using Spark Plasma Sintering: Effect of Mg, Y and La Doping," *J. Eur. Ceram. Soc.*, **30** [3] 1335–43 (2010).
[8]J. Y. Chane-Ching, G. Martinet, P. J. Panteix, C. Brochard, A. Barnabe, and M. Airiau, "Size and Morphology Control of Ultrafine Refractory Complex Oxide Crystals," *Chem. Mater.*, **23** [4] 1070–7 (2011).
[9]C. Li, Y. Imai, Y. Adachi, H. Yamada, K. Nishikubo, and C. N. Xu, "One-Step Synthesis of Luminescent Nanoparticles of Complex Oxide, Strontium Aluminate," *J. Am. Ceram. Soc.*, **90** [7] 2273–5 (2007).
[10]G. Zhan, A. K. Mukherjee, and S. H. Risbud, "Polycrystalline optical window materials from nanoceramics"; US 0011839, 2006.
[11]H. Watanabe and Y. Uchida, "Translucent alumina sintered body and a process for producing the same"; US 6482761, 2002.
[12]L. Lallemant, G. Fantozzi, V. Garnier, and G. Bonnefont, "Transparent Polycrystalline Alumina Obtained by SPS: Green Bodies Processing Effect," *J. Eur. Ceram. Soc.*, **32** [11] 2909–15 (2012).
[13]L. M. Zimmermann and A. F. Silva, "Treatment of Magnesium Ion Adsorption at the Gamma-$Al_2O_3$-Water Interface Quantitative," *J. Phys. Chem. C*, **114** [35] 15078–83 (2010).
[14]M. P. Harmer and R. J. Brook, "Fast Firing – Microstructural Benefits," *J. Br. Ceram. Soc.*, **80** [5] 147–8 (1981).
[15]Y. Aman, V. Garnier, and E. Djurado, "Spark Plasma Sintering Kinetics of Pure α-Alumina," *J. Am. Ceram. Soc.*, **94** [9] 2825–33 (2011).
[16]J. Fang, A. M. Thompson, M. H. Harmer, and H. M. Chan, "Effect of Yttrium and Lanthanum on the Final Stage Sintering Behavior of Ultrahigh Purity Alumina," *J. Am. Ceram. Soc.*, **80** [8] 2005–12 (1997). □